The emergence of large scale magnetic fields in disk galaxies

Xinyu Li
Supervisors: Romain Teyssier, Julien Devriendt, Adrianne Slyz

September 14, 2018

Abstract

In this project, we study whether large scale magnetic fields can emerge from initial small scale field configurations following the galactic dynamics. Using the RAMSES code, we perform MHD simulations on an isolated galaxy. We found that toroidal magnetic fields develop on the disk as a result of galactic rotation. The resulting ordered magnetic component accounts for $10\% - 50\%$ of the total field, which is consistent with observations. Our results suggest that large scale dynamos are not necessary to produce large scale magnetic fields.

1 Introduction

Magnetic fields are ubiquitous in the universe. They have strength revealed by astronomical observations ranging from 10^{-6} G in galaxies up to $10^{12} - 10^{14}$ G in neutron stars. Radio synchrotron emission and Faraday rotational measures provide strong evidence that there are magnetic fields of order $\sim 10^{-5}$ G on the galactic disk [Beck, 2015]. The revealed structure of magnetic fields is correlated with the spiral disks, and the magnetic energy density found to be in equipartition with the turbulent kinetic energy of the gas residing on the disk. Moreover, a significant part the magnetic fields are ordered on the large scale, with the fraction of ordered component $\gtrsim 10\%$ that varies among different galaxies.

How the large scale magnetic fields in disk galaxies are formed is still not fully understood. In the current accepted picture, the magnetic fields are formed in the bottom-up scenario, where initially small scale magnetic fields are amplified and become coherent on large scales. The initial small scale seed fields are generated through the mechanism called "Biermann Battery" [Biermann, 1950]. The cross product of anisotropic electron number density n_e and temperature T contributes a source term to the MHD equation

$$\frac{\partial \boldsymbol{B}}{\partial t} = \nabla \times (\boldsymbol{v} \times \boldsymbol{B}) - \frac{ck_B}{en_e} \nabla n_e \times \nabla T \,. \tag{1}$$

The strength of the seed field is found to be very weak $10^{-20} - 10^{-19}$ G [Subramanian et al., 1994, Gnedin et al., 2000].

The weak seed magnetic fields are amplified through small scale dynamos driven by the galactic motion and feedback. [Rieder and Teyssier, 2016, 2017a] have performed a series of simulations. Their results demonstrated that supernova feedback induces turbulence which drive small scale dynamos and exponentially amplify the magnetic fields. They found that the growth of the magnetic fields saturate when the magnetic energy are in equipartition with the turbulent kinetic energy of the gas. However, the magnetic fields resulting from small scale dynamos are still on small scales. A cosmological simulation following the evolution of high redshift galaxies by [Rieder and Teyssier, 2017b] also found that magnetic fields are mainly on small scales.

Whether the motion of late-time quiescent galaxies is able to lift the small scale magnetic fields to large scales is the main problem we would like to address in this project. We perform MHD simulations on an isolated galaxy to see how large scale magnetic fields can emerge from the galactic motion. Not interested in the early active phase of galaxy formation, we set the initial condition to be a late time disk galaxy already in equilibrium with different magnetic configurations. The details of numerical schemes and initial conditions are presented in Section 2. Analysis and results are presented in Section 3. The final section is devoted to discussion and conclusions.

2 Numerical Schemes

2.1 Description of Methods

We perform MHD simulations of an isolated galaxy using the AMR code RAMSES [Teyssier, 2002] including collisionless particles (stars), gaseous components and magnetic fields. The stars and gaseous components are coupled through gravity. The code solves the ideal MHD equation (cooling and gravity are omitted here for simplicity)

$$\partial_t \rho + \nabla \cdot (\rho \boldsymbol{v}) = 0 \tag{2}$$

$$\partial_t (\rho \boldsymbol{v}) + \nabla \cdot (\rho \boldsymbol{v}\boldsymbol{v}^T - \boldsymbol{B}\boldsymbol{B}^T + P_{\rm tot}) = 0 \tag{3}$$

$$\partial_t E + \nabla \cdot [(E + P_{\rm tot})\boldsymbol{v} - (\boldsymbol{v} \cdot \boldsymbol{B})\boldsymbol{B}] = 0 \tag{4}$$

$$\partial_t \boldsymbol{B} - \nabla \times (\boldsymbol{v} \times \boldsymbol{B}) = 0 \tag{5}$$

where ρ and $\boldsymbol{v}$ are the gas density and velocity, $E = \frac{1}{2}\rho v^2 + \varepsilon + \frac{1}{2}B^2$ is the total energy density with ε being the internal energy density, and $P_{\rm tot} = P + \frac{1}{2}B^2$ is the total pressure with $P = (\gamma - 1)\varepsilon$ following the ideal gas law. The divergence-free condition $\nabla \cdot \boldsymbol{B} = 0$ is guaranteed using the constrained transport method. The code is grid-based with tree-based adaptively refined mesh. MHD equations are solved using the second-order unsplit Gundonov scheme with the HLLD Riemann solver and MinMod slope limiter.

In addition to the MHD equations with gravity, the code also includes the physics of cooling and star formation. The gas cooling is modelled as standard H and He cooling processes based on [Sutherland and Dopita, 1993] for temperature above 10^4 K and [Rosen and Bregman, 1995] for temperature below 10^4 K. The metallicity Z is included in the code as a passive scalar which is initialized as $Z = 0.01 Z_\odot$.

The star formation in the code creates collisionless particles stochastically from gas following the Schimdt law

$$\dot{\rho_*} = \epsilon_* \frac{\rho_{\rm gas}}{t_{\rm ff}} \tag{6}$$

when the local gas density is above the threshold $\rho_* = n_* m_H$ and we set $n_* = 100$ H/cc and $\epsilon_* = 0.01$.

2.2 Isolated Galaxy

We prepare the initial condition of our isolated galaxy using the DICE code [Perret et al., 2014] to study its evolution in the quiescent phase. Our disk galaxy is chosen to be a Milky Way like galaxy with virial mass $M_{200} = 10^{12} M_\odot$. It is composed of a halo including dark matter and gas, an exponential gaseous disk with stars and a stellar bulge. All the matter components are prepared to be in hydrostatic equilibrium with live gravitational field. The gaseous disk has radius $R_d = 15$ kpc with initial temperature 10^4 K. An initial turbulent velocity component with dispersion $\sigma_t = 10$ km/s is injected on the scale of 1 kpc. The galaxy sits on the AMR grid up with resolution up to 100 pc. This resolution is enough to resolve the dynamics of galactic evolution, but not enough for small scale dynamos to be effective.

2.3 Initial Magnetic Fields

The initial magnetic field in our galaxy is composed of a large scale field and small scale random fields. The small scale random fields involve $n = 100$ dipoles centered on the disk plane with random orientations and amplitudes proportional local gas density to mimic the fields resulting from small scale dynamos. The vector potential is given by

$$\boldsymbol{A}_{\text{rand}} = B_{\text{rand}} \sum_i^n \varepsilon^3 \frac{\hat{\boldsymbol{m}}_i \times (\boldsymbol{r} - \boldsymbol{r}_i)}{(|\boldsymbol{r} - \boldsymbol{r}_i| + \varepsilon)^3} \exp\left(-\frac{2r_i}{3R_d}\right) \tag{7}$$

with $\boldsymbol{m}_i$ and $\boldsymbol{r}_i$ being the unit orientation vector and position vector with respect to the disk center for each dipole. B_{rand} is the overall normalization for the amplitude of random dipoles, and a small scale cut off $\varepsilon = 1$ kpc is introduced to avoid the divergence of magnetic field strength.

Moreover, since the small scale dynamo is driven by feedback during the early phase of galactic formation, galactic outflow can uplift the field to the scale of the halo size. Relic large scale magnetic fields could still exist after the gas collapses to form a disk. A quadrupole magnetic configuration, with non-zero radial magnetic flux in the equatorial plane, will have its radial field be amplified on the disk during the collapse. On the contrary, a dipole magnetic configuration with zero radial flux will not be amplified. As a result, the collapse of gas to disk leaves the quadrupole configuration to be the main component of the relic large scale magnetic fields. The vector potential for the large scale quadrupole field sitting at the disk center reads

$$\boldsymbol{A}_{\text{quad}} = B_{\text{quad}} \sum_i^n \varepsilon^3 \frac{\hat{\boldsymbol{z}} \times \boldsymbol{r}}{(|\boldsymbol{r}| + \varepsilon)^3} \exp\left(-\frac{2r_i}{3R_d}\right) . \tag{8}$$

However, the strength of relic quadrupole field is uncertain unless we follow the initial collapse. We employ the approach to perform various simulation runs with different relative strength between the large scale quadrupole field and the small scale dipole field and study the effects.

Table 1: Table of parameters for simulation runs. The amplitude of magnetic is in unit of the saturated value $B_{\rm sat} = \sqrt{\rho\sigma_t^2}$.

Run Name	$B_{\rm quad}$	$B_{\rm rand}$	Star + Cooling	Feedback
Q	10^{-3}	0	No	No
QS	10^{-3}	0	Yes	No
DS	0	10^{-3}	Yes	No
DQS	10^{-3}	10^{-1}	Yes	No
DQSF	N/A	N/A	Yes	Yes

2.4 Simulation Runs

Table 1 lists the parameters for our simulation runs. The nomenclature is chosen such that Q stands for a large scale initial quadrupole field and D for random dipoles, S for star formation and cooling in effect and F for feedback enabled. All simulations end at 750 Myr corresponding to around five rotation periods of the disk.

3 Results

3.1 Disk and Magnetic Field Morphology

Figure 1 plots the gas density and magnetic field lines on the disk viewed from the top at the end of our simulations. The disk in the Q run sustains its initial configuration with spiral arms slowly developed due to the differential rotation. Once star formation and cooling are enabled, the galactic disk fragments to form small clumps with high density. In all runs, large scale magnetic field lines are visible on the plot, and the field lines follow the structure of gas density. When star formation and cooling are turned on, there is no obvious distinction between magnetic field configuration resulting from initial quadrupole (QS) and random dipole fields (DS).

3.2 Growth of the Magnetic Field Energy

The ideal MHD equation for the evolution of magnetic field is given by

$$\frac{\partial \boldsymbol{B}}{\partial t} = \nabla \times (\boldsymbol{v} \times \boldsymbol{B})\,. \tag{9}$$

For an initial condition with purely radial field, as the field is dragged by the rotation, a toroidal field will develop. The toroidal field experiences a linear growth in time during while the radial field remains approximately constant

$$B_\theta \approx B_r \Omega t\,. \tag{10}$$

Therefore, the magnetic field energy is expected to increase proportional to t^2 as opposed to exponential growth from a dynamo.

Figure 2 shows the growth of magnetic energy on the disk normalized by its initial value. The dashed black reference line indicates a growth rate of t^2. For the Q run where the initial magnetic field on the disk is purely radial and without star formation or cooling, its magnetic energy follows the reference

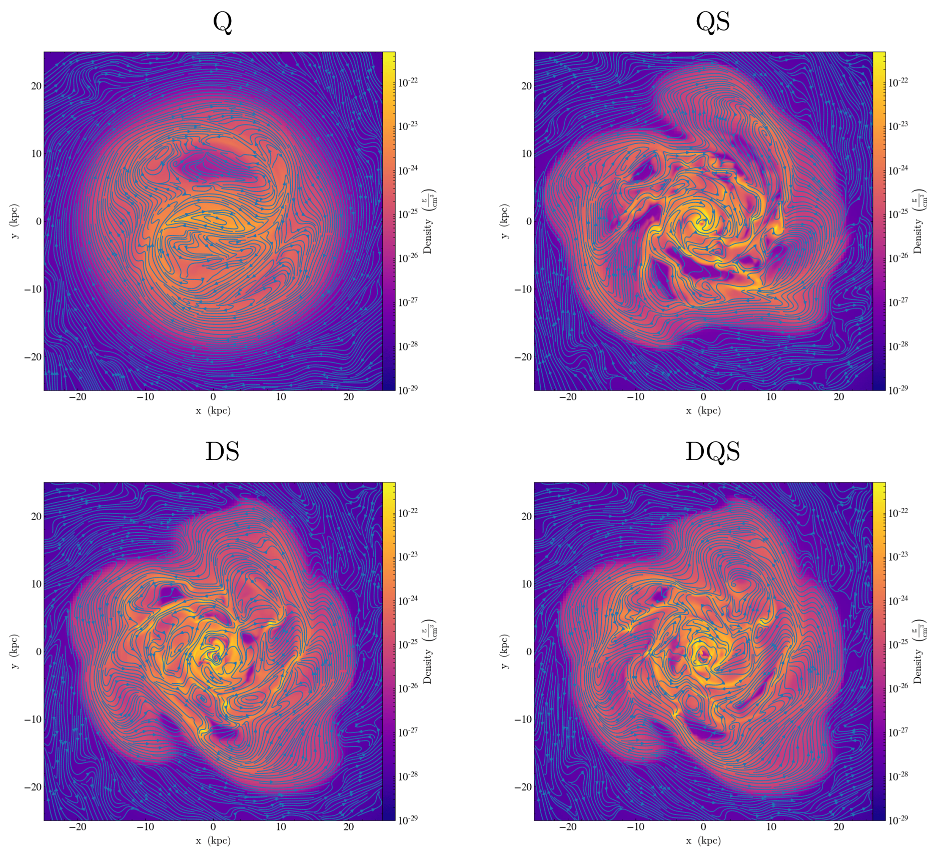

Figure 1: Slice plot of gas density on the disk viewed from the top with magnetic field lines overlaid for various runs.

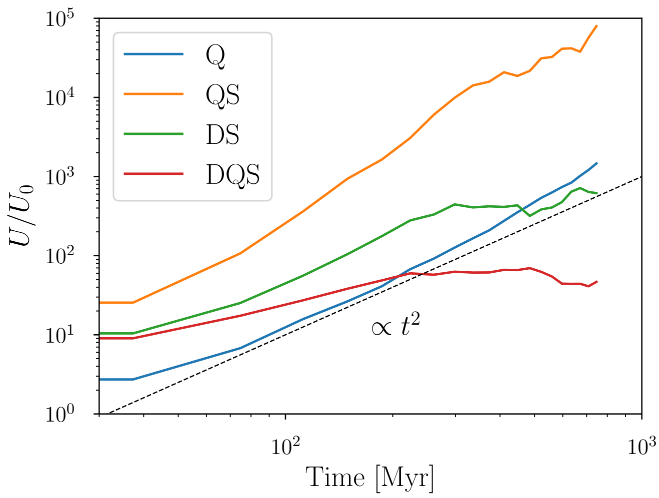

Figure 2: The growth of magnetic energy on the disk.

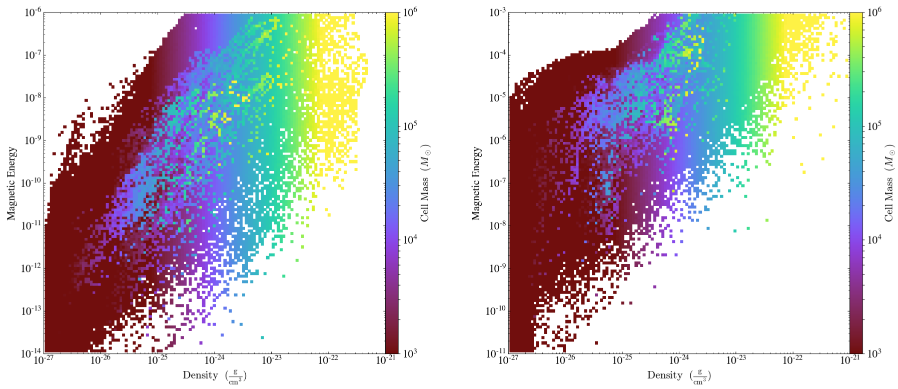

Figure 3: Phase plot for magnetic energy with gas density colored by the cell mass in the simulation. *Left*–QS run, *Right*–DS run. The diagonal line from the left bottom corner to the top right corner follows $B^2 \propto \rho^{4/3}$.

line. Once star formation and cooling are turned on, the collapse of gas to form clumpy structures and stars enhances the growth of magnetic energy as observed by the QS run. Such growth of magnetic field energy also exists for the case of random dipoles in the DS run, which saturates after 300 Myr. The saturation may be due to the finite size of small scale dipoles (~ 1 kpc). The shear motion of the disk stretch the central radial magnetic fields and finally destroy them so that no more growth can be sustained. For the DQS run, the slow growth and saturation is because that the initial magnetic fields are strong. The magnetic fields saturate when they are in equipartition with the turbulent kinetic energy.

To further demonstrate that the enhanced growth of magnetic field is not through dynamos, we plot the phase plot of magnetic energy with gas density. The flux freezing condition from ideal MHD predicts the relation

$$B^2 \propto \rho^{4/3} \tag{11}$$

should be satisfied. Figure 3 shows the phase plot colored by the cell mass at the end of simulations for QS run on the left and DS run on the right. The diagonal line from the left bottom corner to the top right corner follows $B^2 \propto \rho^{4/3}$. Most cells are aligned on the line parallel to the diagonal, indicating they follow the relation given by flux freezing condition.

3.3 Toroidal and order magnetic fields

In Figure 4, we plot the radial profile of large scale toroidal magnetic field on the left with the pitch angle on the right at the end of simulations. A toroidal field as large as 10 μG is observed on the disk for the DQS run with initial condition below the saturation from small scale dynamo. The large toroidal field induces a small magnetic pitch angle on the disk. Especially near the edge the disk, the magnetic pitch angle is close to 0, suggesting that magnetic fields are dominated by the toroidal component.

Reversal of large scale toroidal magnetic fields are observed for all runs except the Q run. The origin of field reversal can be two fold. First, initial random

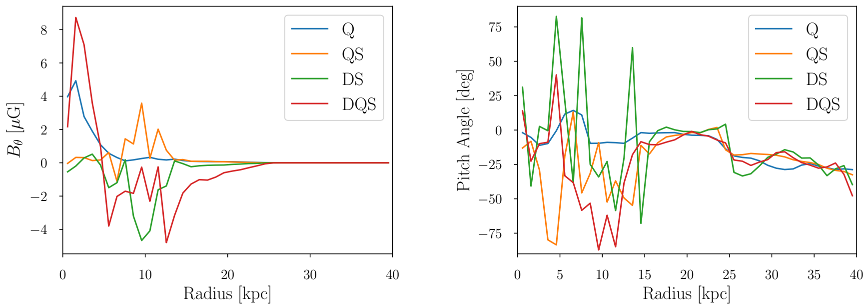

Figure 4: Phase plot for magnetic energy with gas density colored by the cell mass in the simulation. *Left*–QS run, *Right*–DS run. The diagonal line from the left bottom corner to the top right corner follows $B^2 \propto \rho^{4/3}$.

field configuration can imprint its initial field reversal to the large scale fields as seen in DS and DQS run. In addition, star formation and cooling can also create field reversal from highly ordered quadrupole initial field as seen in the QS run. Without star formation and cooling, no field reversal is observed for the Q run.

A large ordered magnetic fraction is also observed in the simulations. Figure 5 plots the radial profile of the ratio of ordered magnetic field over the total. The ordered magnetic is computed by averaging all magnetic fields (B_r, B_θ and B_z) over annuli of 1 kpc thickness. The ratio has magnitude $10 - 60\%$ on the disk indicating that ordered magnetic fields are comparable to the disordered fields.

4 Conclusion and Discussion

We have observed that a large scale magnetic field can emerge from an initially small scale random field configuration. The rotation of the galactic disk is enough to drag the field lines and induce toroidal magnetic components. The resulting magnetic field strength can reach 10 μG, and the fraction of ordered component $\gtrsim 10\%$. They are all consistent with existing observations. Therefore, we may conclude that large scale dynamos are not necessary to create large scale magnetic fields on the galactic disk.

However, we did not include supernova and radiative feedback in our simulations. The feedback will drive small scale turbulence that enables dynamos to work on small scales. Though we don't expect such feedback to be important in our quiescent galaxy, more simulations should be done to demonstrate whether the feedback will destroy the large scale magnetic fields emerging in our simulations which will be our next step.

Moreover, we have tried various initial magnetic configurations including a large scale quadrupole, many small scale dipoles and a mixture of both. To determine the exact initial condition inherited from the early phase of galaxy formation, it would be better to follow the full history of the collapse of the halo. Alternatively, we can tune the relative strength of the quadrupole and small scale dipoles to study their effects on the resulting magnetic fields.

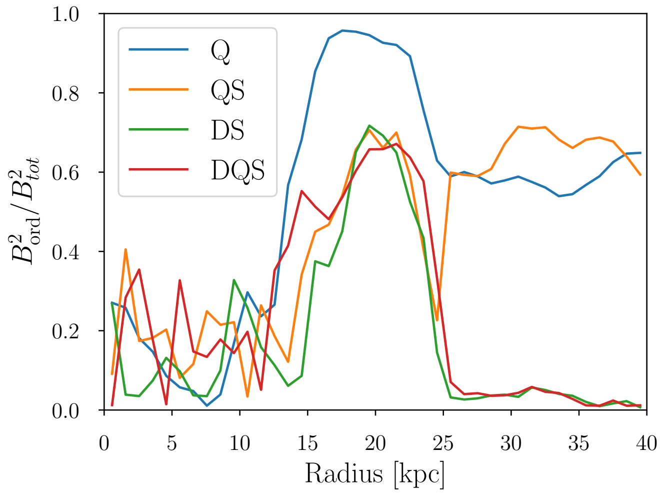

Figure 5: Phase plot for magnetic energy with gas density colored by the cell mass in the simulation. *Left*–QS run, *Right*–DS run. The diagonal line from the left bottom corner to the top right corner follows $B^2 \propto \rho^{4/3}$.

References

Rainer Beck. Magnetic fields in spiral galaxies. *Astronomy and Astrophysics Review*, 24:4, December 2015. doi: 10.1007/s00159-015-0084-4.

L. Biermann. Über den Ursprung der Magnetfelder auf Sternen und im interstellaren Raum. *Zeitschrift Naturforschung Teil A*, 5:65, January 1950.

Nickolay Y. Gnedin, Andrea Ferrara, and Ellen G. Zweibel. Generation of the Primordial Magnetic Fields during Cosmological Reionization. ApJ, 539:505–516, August 2000. doi: 10.1086/309272.

V. Perret, F. Renaud, B. Epinat, P. Amram, F. Bournaud, T. Contini, R. Teyssier, and J.-C. Lambert. Evolution of the mass, size, and star formation rate in high redshift merging galaxies. MIRAGE - A new sample of simulations with detailed stellar feedback. A&A, 562:A1, February 2014. doi: 10.1051/0004-6361/201322395.

Michael Rieder and Romain Teyssier. A small-scale dynamo in feedback-dominated galaxies as the origin of cosmic magnetic fields - I. The kinematic phase. MNRAS, 457:1722–1738, April 2016. doi: 10.1093/mnras/stv2985.

Michael Rieder and Romain Teyssier. A small-scale dynamo in feedback-dominated galaxies - II. The saturation phase and the final magnetic configuration. MNRAS, 471:2674–2686, November 2017a. doi: 10.1093/mnras/stx1670.

Michael Rieder and Romain Teyssier. A small-scale dynamo in feedback-dominated galaxies - III. Cosmological simulations. MNRAS, 472:4368–4373, December 2017b. doi: 10.1093/mnras/stx2276.

Alexander Rosen and Joel N. Bregman. Global Models of the Interstellar Medium in Disk Galaxies. ApJ, 440:634, February 1995. doi: 10.1086/175303.

K. Subramanian, D. Narasimha, and S. M. Chitre. Thermal generation of cosmological seed magnetic fields in ionization fronts. MNRAS, 271:L15, November 1994. doi: 10.1093/mnras/271.1.L15.

Ralph S. Sutherland and M. A. Dopita. Cooling Functions for Low-Density Astrophysical Plasmas. *The Astrophysical Journal Supplement Series*, 88: 253, September 1993. doi: 10.1086/191823.

R. Teyssier. Cosmological hydrodynamics with adaptive mesh refinement. A new high resolution code called RAMSES. A&A, 385:337–364, April 2002. doi: 10.1051/0004-6361:20011817.